

# Quantitative Tissue Characterization Based on Pulsed-Echo Ultrasound Scans

EUGENE WALACH, C. N. LIU, SENIOR MEMBER, IEEE, ROBERT C. WAAG, SENIOR MEMBER, IEEE, AND KEVIN J. PARKER, MEMBER, IEEE

**Abstract**—This paper describes a novel technique for estimating ultrasonic attenuation coefficients. The technique first employs a histogram analysis to estimate the number of tissues present and then utilizes a maximum likelihood criterion to assign attenuation values, thus producing an image of attenuation. Simulated *B*-scan data and clinical *B*-scan data are used to illustrate the method. The results show that images representing an intrinsic tissue parameter can be produced when the basic model is valid.

## I. INTRODUCTION

ULTRASONIC imaging has already had a major impact on diagnosis in medicine. However, current clinical imaging techniques and computer image enhancements produce only qualitative images which require experience for interpretation [1]. The purpose of this paper is to describe a new method for estimating the tissue attenuation coefficient based entirely on conventional ultrasonic *B*-scan measurements [2].

We will assume a simple exponential model for the backscatter echo amplitude from the *i*th pulse of a sector scan [3]–[6]:

$$E_i(x) = \frac{E_0}{x} \sigma_i(x) \exp \left[ -2 \int_0^x \alpha_i(r) dr \right] \quad (1)$$

where  $\sigma$  represents the scattering coefficient,  $x$  represents the (nonzero) distance to the transducer,  $\alpha$  stands for the attenuation coefficient, and  $E_0$  is a constant of proportionality. The factor of two in the exponent in (1) arises from the roundtrip to the reflector and back to the transducer. In our model, transducer beam width and pulse length effects, which produce amplitude fluctuations sometimes called speckle or texture [7], [8], are represented by the assumption that the backscatter echo amplitude is a random variable.

By sampling both sides of (1), the measured data can

Manuscript received June 6, 1985. This work was supported in part by NSF Grants ECS 80 17683 and ECS 84 14315, NIH Grant CA 39516, NATO Grant 93 81, and the Diagnostic Ultrasound Research Laboratory Industrial Associates.

E. Walach was with the IBM T. J. Watson Research Center, Yorktown Heights, NY 10598. He is now with the IBM Haifa Scientific Center, Haifa, Israel.

C. N. Liu is with the IBM T. J. Watson Research Center, Yorktown Heights, NY 10598.

R. C. Waag and K. J. Parker are with the Departments of Electrical Engineering and Diagnostic Radiology, University of Rochester, Rochester, NY 14642.

IEEE Log Number 8608288.

be represented as a system of nonlinear equations—one equation for every time sample, which in turn corresponds to a certain picture element (pel):

$$E_{ij} = \frac{E_0}{x_{ij}} \sigma_{ij} \exp \left[ -2 \sum_j \alpha_{ij} \right] \quad (2)$$

where  $E_{ij}$  is the amplitude of the echo received from the pel *ij* (the *i*th interrogation of the *j*th sample volume),  $\sigma_{ij}$  and  $\alpha_{ij}$  are backscattering and attenuation coefficients, respectively, and the summation is performed along the path of the ultrasonic ray. By simply taking logarithms of both sides, one can rewrite (2) as a system of linear equations

$$\ln E^* = \ln E_0 \sigma - 2A\alpha \quad (3)$$

where  $E^*$  stands for the vector of measured echo samples (multiplied by corresponding distances to the transducer),  $\sigma$  and  $\alpha$  are vectors of backscattering and attenuation coefficients, and  $A$  is a matrix (with entries 0 or 1) determined by the geometry of the problem. A *B*-scan image provides the values for the left side of (3). The matrix  $A$  is known from the experimental setup. The goal is to find  $\sigma$  and  $\alpha$ .

Assume for convenience and without loss of generality that the image is square of size  $N \times N$ . Hence, the system of equations (3) will have  $2N^2$  unknowns (backscatter and attenuation coefficients for every pel of the image) and  $pN^2$  equations where  $p$  is the number of different projections of the area under consideration. Naturally, the existence of a unique solution to (3) is contingent on the problem being nonsingular. This means that  $p$  has to be at least not smaller than two [3]. Unfortunately, in most practical cases, even a relatively large  $p$  does not ensure a reasonable estimation of  $\sigma$  and  $\alpha$ . Indeed, in most practical cases, the eigenvalue spread associated with the system of equations (3) is extremely high. Moreover, the signal-to-noise ratio of the ultrasonic data is quite low [7], [8]. Consequently, large computational artifacts may distort an image of attenuation and backscatter coefficient [3]. In order to resolve this issue, one has to redefine the mathematical formulation of the problem so that the number of degrees of freedom will be reduced. Fortunately, since the biological object to be imaged may consist of a relatively small number of uniform tissues, we can often find regions of constant  $\sigma$  and then estimate the corresponding  $\alpha$ .

In this paper, we will first describe a way to determine

the number of different tissues present in any given image. Then we develop a way to partition the image into a number of mutually exclusive areas—one area for every tissue present. Once such a partition is achieved, we proceed to compute an attenuation coefficient for every tissue area using a maximum likelihood algorithm. Finally, three examples are presented in order to illustrate the performance of the approach.

## II. STATISTICAL CHARACTER OF THE ULTRASONIC ECHO AMPLITUDES

Consider first the distribution of the echo amplitudes received from a statistically homogeneous region of randomly positioned scatterers. As already observed, despite the homogeneity of the region of interest, one can expect amplitude fluctuations which arise from within the resolution cell formed by the beam width and pulse length as the transducer is scanned through the region of interest. When the number of scatterers within one resolution element (pel) is large and the phases of the scattered waves are uniformly distributed between 0 and  $2\pi$ , the ultrasonic echo amplitude, as noted by previous investigators [7], [8], will have a Rayleigh distribution:

$$p(v) = \frac{v}{s} e^{-v^2/2s} \quad v \geq 0$$

$$= 0 \quad v < 0 \quad (4)$$

where  $v$  stands for the echo amplitude,  $p$  is the probability distribution, and  $s$  is a constant called the Rayleigh coefficient which can be expressed in terms of the mean by the relation  $E[v] = (\pi s/2)^{1/2}$ .

Next consider a more realistic case in which the object consists of a number of different tissues. Each tissue will have different backscattering properties, i.e., different Rayleigh coefficients. Hence, the overall probability distribution will consist of a number of superimposed Rayleigh distributions.

The first question is how many different tissues are present in any given image and what are the corresponding Rayleigh coefficients. An experienced physician might have an immediate answer to this question based on the knowledge of the anatomical structure of the imaged target and accumulated statistics of the previous studies. However, in this investigation, we will proceed under the assumption that no such *a priori* knowledge is available. Hence, this issue must be resolved by the analysis of the image itself.

The Rayleigh probability distribution function has a single peak located exactly at the square root of the corresponding Rayleigh coefficient. The histogram of the image of a nonhomogeneous object will have a number of peaks. The number of different tissues present will be equal to the number of such peaks and each peak implies a Rayleigh coefficient.

This observation suggests a simple procedure for finding the Rayleigh coefficients of the various tissues present in a given image from histograms. The preparation of a histogram requires a choice of a single arbitrary parame-

ter: "the interval" or "cell size" [9]. Following [9], we choose the cell width as twice the interquartile range of data divided by the cube root of the sample size. In our experience, this rule proved to be very efficient and useful.

Once the number and character (Rayleigh coefficients) of all the tissues present have been established, it is possible to decide to which tissue every pel belongs. As a decision rule, we have adopted the principle of maximum likelihood which is known to have certain optimality qualities [10].

Assume that we have established the existence of the  $K$  different tissues with the corresponding Rayleigh coefficients being  $S_1, \dots, S_K$ . We wish to "assign" the pel  $ij$  which resulted in the echo  $E_{ij}$  to one of the possible tissues. Thus, we compute the probabilities

$$P_k = \frac{E_{ij}}{S_k} e^{-E_{ij}^2/2S_k} \quad K \geq k \geq 1. \quad (5)$$

Each number  $P_k$  provides the probability of obtaining the echo  $E_{ij}$  from the pel belonging to the tissue number  $k$ . The maximum likelihood principle assigns the pel  $ij$  to the tissue  $k$  which has the highest probability:

$$P_k = \max \{P_1, \dots, P_K\}. \quad (6)$$

Introducing a spatial filtering to reduce the error of assigning the pels, we obtain the following algorithm.

- 1) Choose a window  $W_{ij}$  which will include all the pels which are relevant to the tissue assignment of the pel  $ij$ .
- 2) Assign weight  $t_r$  to every pel  $r$  inside this window.
- 3) For every  $K \geq k \geq 1$  and every pel in the window, compute the probability  $p_{rk}$  of obtaining echo  $E_r$  if pel  $r$  belonged to the tissue  $k$ .
- 4) Compute

$$p_k = \prod_{W_{ij}} p_{rk}^{t_r}. \quad (7)$$

- 5) Use the maximum likelihood principle, i.e., assign pel  $ij$  to the tissue which resulted in the maximum probability  $p_k$ .

In our simulations, we have chosen small windows of  $3 \times 3$  or  $5 \times 5$  pels (which correspond roughly to the resolution which is about 1 mm in the axial direction along the wave and 3 mm in the lateral dimension) and assigned the uniform weight ( $t_r = 1$ ) to every pel inside the window.

## III. ESTIMATION OF THE TISSUE ATTENUATION COEFFICIENT

For practical reasons, let us assume that the tissues are independent from each other and that the data can be represented in the form depicted in Fig. 1. The tissue under consideration is crossed by a number  $P$  of ultrasonic rays. Each ray  $i$ ,  $P \geq i \geq 1$ , contributes a block of  $k_i$  pels which are located inside the tissue. We will denote the echos of the block number  $i$  as  $E_{i1}, E_{i2}, \dots, E_{iki}$ . Since we do not know what was the impact of the path passed before each ray arrived at the area of interest, we have to

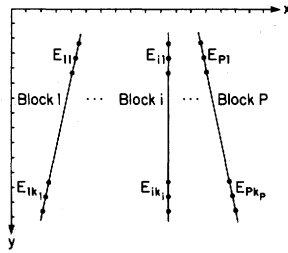


Fig. 1. Schematic structure of the data.

assume that each block may start at some arbitrary level  $E_i$ . However, from that point on, all the echos from all the blocks are assumed to follow an exponential dependence on the same attenuation coefficient  $\alpha$ . Hence, for every tissue, we will have, to begin with,  $\sum_{i=1}^P k_i$  data samples (equations) in  $P + 1$  unknowns. Our goal is to find an attenuation coefficient which will minimize a certain cost function.

Assume for the moment that we know the value of the attenuation coefficient  $\alpha$  and a known accumulated attenuation  $A_i$  for every block  $i$ . Then compensate each echo sample for the attenuation effect. The compensated echo from the pel  $ij$  will have the value

$$A_i E_{ij} e^{2(j-1)\alpha}. \quad (8)$$

The probability of obtaining this value from the tissue with the Rayleigh coefficient  $s$  is

$$p_{ij} = \frac{A_i E_{ij} e^{2(j-1)\alpha}}{s} \exp \left[ -\frac{A_i^2 E_{ij}^2 e^{4(j-1)\alpha}}{2s} \right]. \quad (9)$$

Assuming that all the data samples are independent of each other, the overall probability of obtaining the existing set of measurements is

$$C = \prod_{i=1}^P \prod_{j=1}^{k_i} p_{ij}. \quad (10)$$

The maximum likelihood principle requires the choice of  $\alpha$  and  $A_i$ ,  $P \geq i \geq 1$ , such that probability (10) will be maximized. Maximizing  $C$  is equivalent to the maximization of

$$\begin{aligned} \ln C &= \sum_{i=1}^P \sum_{j=1}^{k_i} \ln p_{ij} \\ &= \ln C_0 + \sum_{i=1}^P \sum_{j=1}^{k_i} \ln A_i \\ &\quad + 2(j-1)\alpha - \frac{A_i^2 E_{ij}^2}{2s} e^{4(j-1)\alpha} \end{aligned} \quad (11)$$

where  $C_0$  is a constant independent of  $A_i$ ,  $P \geq i \geq 1$ , and  $\alpha$ . Equating to zero the derivative of (11) relative to  $A_i$  yields for every  $P \geq i \geq 1$

$$\frac{A_i^2}{s} = \frac{k_i}{\sum_{j=1}^{k_i} E_{ij}^2 e^{4(j-1)\alpha}}. \quad (12)$$

Finally, equating to zero the derivative of (11) relative to the  $\alpha$  and substituting (12) yields the "optimality" condition

$$0.5 \sum_{i=1}^P k_i (k_i - 1) = \sum_{i=1}^P \frac{k_i \sum_{j=1}^{k_i} E_{ij}^2 (j-1) e^{4(j-1)\alpha}}{\sum_{j=1}^{k_i} E_{ij}^2 e^{4(j-1)\alpha}}. \quad (13)$$

Equation (13) is nonlinear in  $\alpha$ . In order to obtain a closed expression for  $\alpha$ , we will assume that the attenuation coefficient is small (relative to the unity), and therefore all the exponentials in (13) can be approximated by the first two terms in the Taylor series expansion. Hence, (13) yields

$$\alpha = \frac{\sum_{i=1}^P NO_i}{\sum_{i=1}^P DN_i} \quad (14)$$

where

$$NO_i = 0.5k_i(k_i - 1) - k_i \frac{b_i}{a_i} \quad (15)$$

$$DN_i = 4k_i \frac{c_i a_i - b_i^2}{a_i^2} \quad (16)$$

and

$$\begin{aligned} a_i &= \sum_{j=1}^{k_i} E_{ij}^2 \\ b_i &= \sum_{j=1}^{k_i} (j-1) E_{ij}^2 \\ c_i &= \sum_{j=1}^{k_i} (j-1)^2 E_{ij}^2. \end{aligned} \quad (17)$$

Utilizing (14)–(17), the estimated value of the tissue attenuation coefficient can easily be computed. Moreover, since the bulk of computations is performed independently for every block of data, our algorithm can be easily implemented on a parallel processor for maximum speed. The accuracy of this algorithm is analyzed in the Appendix.

#### IV. EXAMPLES AND DISCUSSION

A  $B$ -scan image model which consists of two oval cysts on uniform background is shown in Fig. 2. The Rayleigh coefficient of the right-hand cyst was chosen to be one. The choice for the left-hand cyst and for the background was 10 000 and 100, respectively. Attenuation coefficients were chosen to be 0, 0.01, and 0.0025 neper/pel, respectively. The  $B$ -scan image was created by drawing independent amplitude samples from the pools of random values having Rayleigh distributions with the chosen coefficients. The attenuation effects were simulated by multiplying each amplitude value by the integral of the attenuation along the ray path. The procedure described in the last section was used to estimate the tissue attenuation

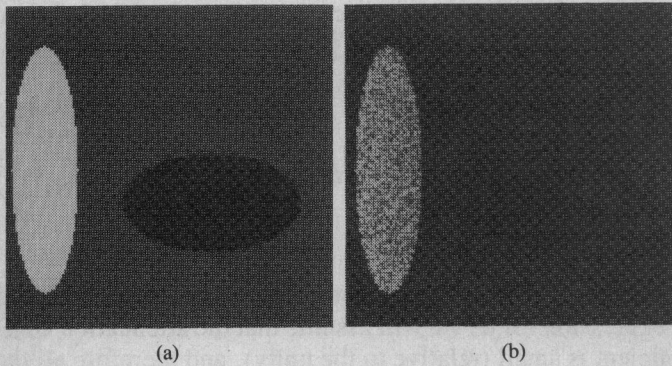


Fig. 2. Simulated *B* scan (b) of an object (a).

TABLE I

ESTIMATED ATTENUATION COEFFICIENT OF THE SIMULATED TARGET

Attenuation Coefficient	Area		
	Right Cyst	Left Cyst	Background
True Value	0	0.01	0.0025
Estimation	0.0003	0.0095	0.0026
Error	0.00028	0.0008	0.0002

coefficients for this simulated *B*-scan image. The results are presented in the Table I. In this case, clearly, the estimated values (the second row) constitute an excellent approximation of the actual values (the first row). The third row of Table I presents our estimation of an error (the square root of the variance). Note that the lowest error can be expected for the background which has the largest area. On the other hand, the right-hand cyst has a smaller area and has a correspondingly larger estimation error. However, since the scan direction is from left to right, this cyst includes long data blocks. Hence, estimated error remains relatively low. Finally, the left-hand cyst has the worst error which reflects small area and relatively short data blocks. In all three cases, the actual estimation error was well within reasonable expectations.

Next, the procedure was applied to *B* scans of human liver. The *B* scans were obtained using an Octoson imaging instrument in a way previously described [2], [11]. Basically, backscattered RF waveforms were digitized and stored along with beam position information and time-varying gain settings. During subsequent digital processing, the waveforms were envelope detected and then the effects of time-varying gain and amplifier compression were removed. No correction for beam diffraction was employed because the effect of diffraction was known to vary amplitudes less than 10 percent throughout the 6 cm interval surrounding the transducer focus which was situated centrally in the livers being studied.

A *B*-scan image of a normal liver is shown in Fig. 3. After the waveforms used to construct this image were decompressed, a histogram of the amplitudes was obtained. An analysis of this histogram indicated that six different regions of tissue were present. Our computation of attenuation for each region produced the image pre-

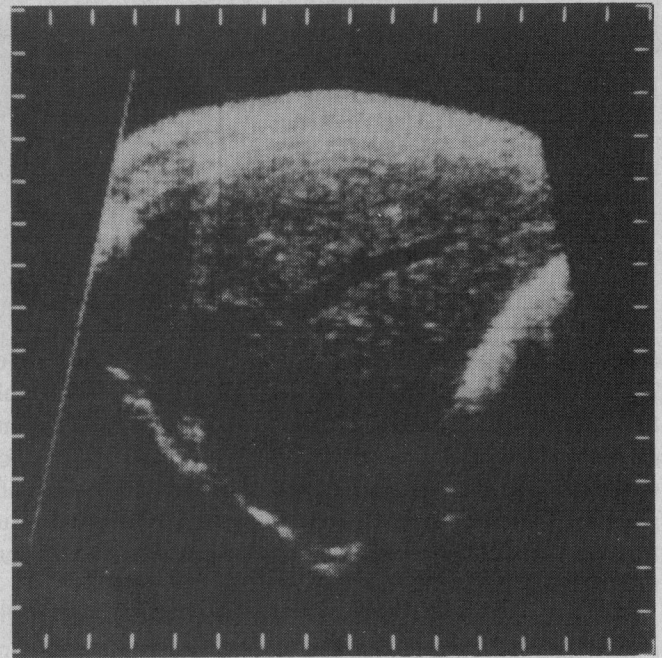


Fig. 3. Digitized clinical *B* scan of a normal liver.

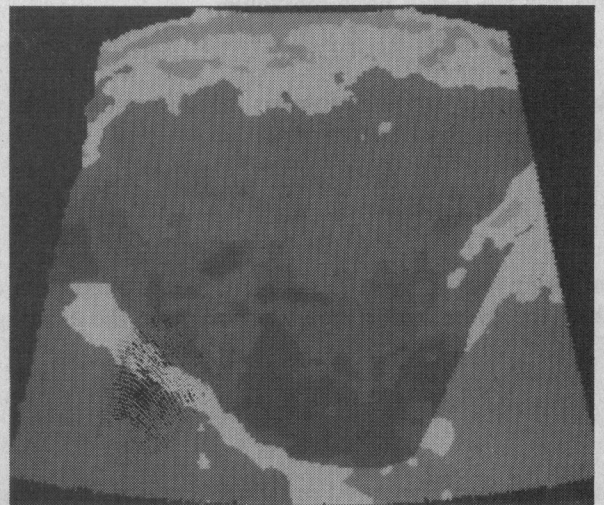


Fig. 4. Attenuation imaging computed from echos in Fig. 3.

sented in Fig. 4. In this image, a linear gray scale is used to represent attenuation in decibels with black equal to 0 dB/cm and white equal to 4.5 dB/cm. High attenuation (about 1.75 dB/cm) was found near the edges of the liver, while the interior of the liver is relatively homogeneous with attenuation in the range of 0.6–0.8 dB/cm. The values in the interior are comparable to a value of 1.0 dB/cm found at 2 MHz by a spectral decay method treated elsewhere [2], [11] and the high attenuation values surrounding the liver are attributed to boundary effects.

In Fig. 5 is a *B* scan of a liver known to have high ultrasonic attenuation. Waveform decompression, amplitude histogram analysis, and partitioning into six different tissue regions for this study produced the image of attenuation given in Fig. 6 for which the gray scale assignments are the same as those in Fig. 4. The attenuation for

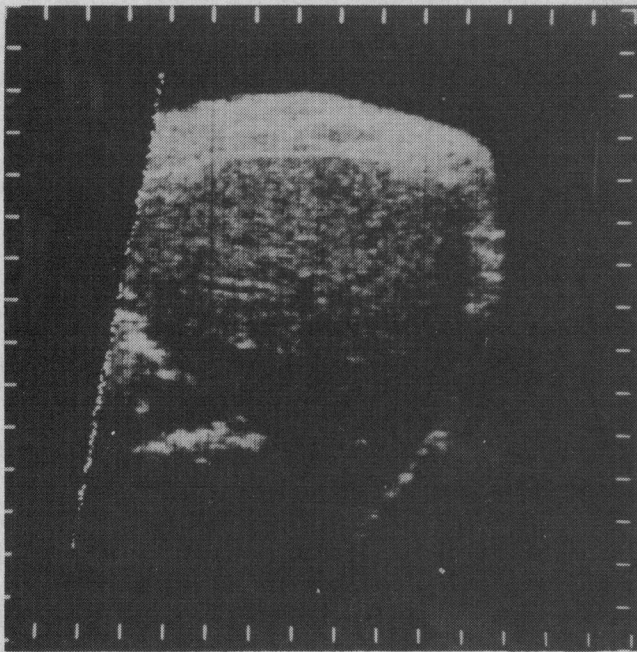


Fig. 5. Digitized clinical B scan with high attenuation.

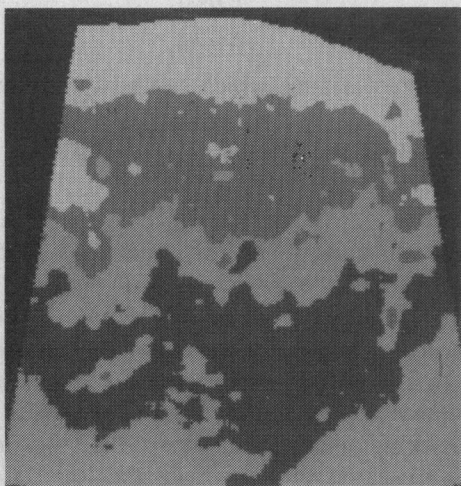


Fig. 6. Attenuation imaging computed from Fig. 5.

a broad central area below the abdominal wall is 1.3 dB/cm, which is the same as that given for the region at 2 MHz by a spectral decay method.

Banding of attenuation with range is evident to different degrees in Figs. 4 and 6. This banding is not thought to be a consequence of liver structure. Rather, the banding is thought to arise from a combination of factors which include beam diffraction, imperfect amplifier decompression, and poor signal-to-noise ratio in posterior regions.

While the specific influence of various factors merits additional investigation, our results illustrate a new way that quantitative ultrasonic images may be obtained from conventional pulsed-echo measurements.

#### APPENDIX

The purpose of this Appendix is to evaluate the estimation error which can be expected while computing the

tissue attenuation coefficient from the expressions (14)–(17). Our aim is to establish a simple approximation of the error of estimation based on a single block of  $K$  data samples  $T_1, T_2 e^{-2\alpha}, \dots, T_K e^{-2(K-1)\alpha}$  where  $T_1, T_2, \dots, T_K$  are mutually independent random variables obeying the Rayleigh distribution with the Rayleigh coefficient equal to a certain positive number  $s$ . In order to achieve this result, certain simplifying assumptions and approximations are required. However, despite this heuristic nature of our derivation, there is an excellent agreement between the theory and the simulation results.

Utilizing expressions (14)–(17) for a single block of  $K$  data samples yields the following expression for the estimated attenuation coefficient  $\tilde{\alpha}$  as a function of the actual attenuation coefficient  $\alpha$ :

$$\tilde{\alpha} = \frac{(K-1)a(\alpha) - 2b(\alpha)}{8\left(c(\alpha) - \frac{b^2(\alpha)}{a(\alpha)}\right)} \quad (\text{A.1})$$

where

$$\begin{aligned} a(\alpha) &= \sum_{j=1}^K T_j^2 e^{-4(j-1)\alpha} \\ b(\alpha) &= \sum_{j=1}^K T_j^2 (j-1) e^{-4(j-1)\alpha} \\ c(\alpha) &= \sum_{j=1}^K T_j^2 (j-1)^2 e^{-4(j-1)\alpha} \end{aligned} \quad (\text{A.2})$$

Expanding (A.1) in the Taylor series around  $\alpha = 0$  yields

$$\tilde{\alpha} = f_0 + f_1\alpha + f_2\alpha^2 + \dots \quad (\text{A.3})$$

For small attenuation coefficient  $\alpha$ , the error resulting from the high-order terms is negligible. Hence, we will concentrate only on the error introduced by the first bias term  $f_0$ . By examining (A.1), we can express the bias term as

$$f_0 = \frac{N_0}{D_0} \quad (\text{A.4})$$

where

$$\begin{aligned} N_0 &= (K-1)a(0) - 2b(0) \\ D_0 &= 8\left(c(0) - \frac{b^2(0)}{a(0)}\right) \end{aligned} \quad (\text{A.5})$$

Consider individually the behavior of the numerator  $N_0$  and the denominator  $D_0$ . For the large values of  $K$ , the denominator will be also large and we have

$$E[a(0)] = E\left[\sum_{j=1}^K T_j^2\right] = E[T_j^2] \sum_{j=1}^K 1 = 2Ks \quad (\text{A.6})$$

$$\begin{aligned} E[b(0)] &= E\left[\sum_{j=1}^K T_j^2 (j-1)\right] = E[T_j^2] \sum_{j=1}^K (j-1) \\ &= K(K-1)s \end{aligned} \quad (\text{A.7})$$

$$E[c(0)] = E \left[ \sum_{j=1}^K T_j^2 (j-1)^2 \right] = E[T_j^2] \sum_{j=1}^K (j-1)^2$$

$$= \frac{s}{3} K(K-1)(2K-1) \quad (\text{A.8})$$

$$E[b^2(0)] = E \left[ \sum_{j=1}^K T_j^4 (j-1)^2 + \sum_{j=1}^K T_j^2 \sum_{\substack{i=1 \\ i \neq j}}^K T_i^2 (i-1) \right]$$

$$= \left( E[T_j^4] \sum_{j=1}^K (j-1)^2 + E[T_j^2]^2 \right. \\ \left. \cdot \left( \sum_{j=1}^K (j-1) \sum_{\substack{i=1 \\ i \neq j}}^K (i-1) \right) \right)$$

$$= \frac{s^2}{3} K(K-1)(3K^2 + K - 2). \quad (\text{A.9})$$

Substituting into (A.4) the corresponding expected values instead of  $a(0)$ ,  $b^2(0)$ , and  $c(0)$ , we can express the denominator as

$$D_0 \cong 8 \left( \frac{s}{3} K(K-1)(2K-1) - \frac{s}{6} K(K-1) \right. \\ \left. \cdot (3K^2 + K - 2) \right) \cong \frac{4s}{3} K^3. \quad (\text{A.10})$$

On the other hand, for small values of  $K$ , the denominator will be very small. Thus, according to (A.6) and (A.7), we have

$$E[N_0] = (K-1) E[a(0)] - 2E[b(0)] = 0. \quad (\text{A.11})$$

However, the numerator will have a nonzero variance:

$$E[N_0^2] = (K-1)^2 E[a^2(0)] - 4(K-1) \\ \cdot E[a(0) b(0)] + 4E[b^2(0)]. \quad (\text{A.12})$$

In order to evaluate the expression (A.12), we note

$$E[a^2(0)] = \sum_{j=1}^K T_j^4 + \sum_{j=1}^K \sum_{\substack{i=1 \\ i \neq j}}^K T_j^2 T_i^2$$

$$= 8s^2 K + 4s^2 K(K-1) = 4s^2 K(K+1) \quad (\text{A.13})$$

and

$$E[a(0) b(0)] = E \left[ \sum_{j=1}^K T_j^4 \right] + E \left[ \sum_{j=1}^K T_j^2 \sum_{\substack{i=1 \\ i \neq j}}^K T_i^2 (i-1) \right]$$

$$= \left( E[T_j^4] \sum_{j=1}^K (j-1) \right) + (E[T_j^2])^2 \\ \cdot \sum_{j=1}^K \sum_{\substack{i=1 \\ i \neq j}}^K (i-1)(j-1)$$

$$= s^2(4K(K-1) + 2K(K-1)^2)$$

$$= 2s^2 K(K^2 - 1). \quad (\text{A.14})$$

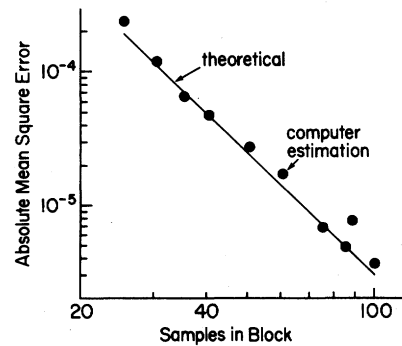


Fig. 7. Dependence of estimation error on the length of data block.

Substitution of (A.9), (A.13), and (A.14) into (A.12) yields

$$E[N_0^2] = \frac{4s^2}{3} (K-1) K(K+1) \cong \frac{4s^2}{3} K^3. \quad (\text{A.15})$$

Hence, we conclude that for a small attenuation coefficient  $\alpha$  and for a large block length  $K$ , the bias term  $f_0$  will have a small mean value, i.e.,

$$f_0 \cong \frac{E[N_0]}{E[D_0]} = 0 \quad (\text{A.16})$$

and a nonzero variance which can be approximated as

$$E[f_0^2] \cong \frac{E[N_0^2]}{E[D_0^2]} \cong \frac{E[N_0^2]}{(E[D_0])^2} \cong \frac{3}{4K^3}. \quad (\text{A.17})$$

In order to verify the expression (A.17), a computer simulation was performed. The attenuation coefficient was computed utilizing expression (A.1) for blocks of data varying in length from 25 to 100 samples. The error between the actual and estimated attenuation coefficients was computed. The process was repeated 100 times, each time with a totally independent data set. Then the mean-square error was computed as a function of the block length. The result is presented in Fig. 7. In the log-log scale, the expression (A.17) takes the form of the straight line. The circles represent the mean-square error measured from the simulation. Despite some crude approximations which had been adopted in our derivations, an excellent agreement between the theoretical and experimental results can be observed.

#### ACKNOWLEDGMENT

The authors acknowledge help from Dr. R. Gramiak and Dr. R. M. Lerner for useful discussions of the results.

#### REFERENCES

- [1] C. N. Liu, M. Fatemi, and R. C. Waag, "Digital processing for improvement of ultrasonic abdominal images," *IEEE Trans. Med. Imaging*, vol. MI-2, pp. 66-75, June 1983.
- [2] K. J. Parker and R. C. Waag, "Measurement of ultrasonic attenuation within regions selected from B-scan images," *IEEE Trans. Biomed. Eng.*, vol. BME-30, pp. 431-437, Aug. 1983.
- [3] E. J. Farrell, "Backscatter and attenuation imaging from ultrasonic scanning in medicine," *IBM J.*, vol. 26, pp. 746-758, Nov. 1982.
- [4] F. A. Duck and C. R. Hill, "Acoustic attenuation reconstruction from backscattered ultrasound," in *Computer Aided Tomography and Ul-*

*trasonics in Medicine*, J. Raviv, J. F. Greenleaf, and G. T. Herman, Eds. Amsterdam: North-Holland, 1979.

- [5] R. W. Rowe, "Ultrasonic image reconstruction," IBM U.K. Sci. Cen., Winchester, England, Rep. UKSC 107, 1981.
- [6] J. F. Havlice and J. C. Taenzer, "Medical ultrasonic imaging: An overview of principles and instrumentation," *Proc. IEEE*, vol. 67, pp. 620-641, Apr. 1979.
- [7] C. B. Burckhardt, "Speckle in ultrasound B-mode scans," *IEEE Trans. Son. Ultrason.*, vol. SU-25, pp. 1-6, Jan. 1978.
- [8] R. F. Wagner, S. W. Smith, and H. Lopez, "Statistics of speckle in ultrasound B-scans," *IEEE Trans. Son. Ultrason.*, vol. SU-30, pp. 156-163, May 1983.
- [9] D. Freedman and P. Diaconis, "On the histogram as a density estimator: L2 theory," *Z. Wahrscheinlichkeitstheorie verw. Gebiete*, vol. 57, pp. 453-476, 1981.
- [10] G. C. Goodwin and R. L. Payne, *Dynamic System Identification: Experiment Design and Data Analysis*. New York: Academic, 1977.
- [11] K. J. Parker, R. M. Lerner, and R. C. Waag, "Attenuation of ultrasound: Magnitude and frequency dependence for tissue characterization," *Radiology*, vol. 153, pp. 785-788, Dec. 1984.



**Eugene Walach** was born in Lvov, U.S.S.R., on February 2, 1952. He received the B.Sc., M.Sc., and D.Sc. degrees in electrical engineering, from the Technion-Israel Institute of Technology, Haifa, in 1973, 1975, and 1981, respectively.

During the years 1981-1983 he was with the Information System Laboratory, Stanford University, as a Chaim Weizmann Postdoctoral Fellow. In 1983-1984 he was a Visiting Scientist at the IBM T. J. Watson Research Center, Yorktown Heights, NY. He is currently a staff member of

the IBM Israel Scientific Center, Haifa, Israel. His research interests are in the areas of image and signal processing, adaptive systems, and analysis of multivariable systems.

Dr. Walach is a member of Sigma Xi.



**C. N. Liu** (M'67-SM'83) received the Ph.D. degree in electrical engineering from the University of Illinois, Chicago, in 1961.

He is currently a Research Staff Member and the Manager of Image Construction and Presentation Systems in the Computer Sciences Department of the IBM T. J. Watson Research Center, Yorktown Heights, NY, responsible for the research and advanced development of image/graphics systems for engineering/scientific applications. From 1978 to 1981 he was Manager of

Medical Ultrasound, engaging in the development of computer techniques for extracting quantitative diagnostic information from pulsed-echo ultrasound scans. From 1961 to 1977 he worked on a number of projects involving the development of pattern recognition and image processing tech-

niques and systems. From 1968 to 1969 he was on leave from IBM Research as a Visiting Associate Professor at the School of Electrical Engineering, Purdue University, Lafayette, IN. His current research interests include engineering and scientific image/graphics workstations, image processing, and pattern recognition systems.

Dr. Liu is a member of the Association for Computing Machinery.



**Robert C. Waag** (S'59-M'66-SM'83) was born in Upper Darby, PA, in 1938. He received the B.E.E., M.S., and Ph.D. degrees from Cornell University, Ithaca, NY, in 1961, 1963, and 1965, respectively.

After completing his Ph.D. studies, he became a member of the Technical Staff at the Sandia Laboratories, Albuquerque, NM, and then served in the United States Air Force from 1966 to 1969 at the Rome Development Center, Griffiss Air Force Base, NY. In 1969 he joined the faculty at the

University of Rochester, Rochester, NY, where he is now a Professor in the Department of Electrical Engineering, College of Engineering and Applied Science, and also holds an appointment in the Department of Radiology, School of Medicine and Dentistry. His recent research has dealt with computer-based processing of ultrasonic signals and the use of ultrasonic scattering for determination of tissue characteristics.

Dr. Waag is a Fellow of the American Institute of Ultrasound in Medicine and a member of the Acoustical Society of America and the Association for Computing Machinery.



**Kevin J. Parker** (S'79-M'81) was born in Rochester, NY, in 1954. He received the B.S. degree in engineering science, *summa cum laude*, from S.U.N.Y., Buffalo, in 1976, and the M.S. and Ph.D. degrees in electrical engineering and biomedical ultrasonics from M.I.T., Cambridge, in 1978 and 1981, respectively.

From 1981 to 1985 he was an Assistant Professor of Electrical Engineering at the University of Rochester; currently he holds the title of Associate Professor. His research interests are in

ultrasonic tissue characterization, medical imaging, and general linear and nonlinear acoustics.

Dr. Parker was the recipient of a National Institute of General Medical Sciences Biomedical Engineering Fellowship (1979), Lilly Teaching Fellowship (1982), and Whitaker Foundation Biomedical Engineering Grant Award (1983). He serves as Chairman of the Rochester Section of the IEEE Engineering in Medicine and Biology Society, a member of the IEEE Sonics and Ultrasonics Symposium Technical Committee, and as reviewer and consultant for a number of journals and institutions. He is also a member of the Acoustical Society of America.